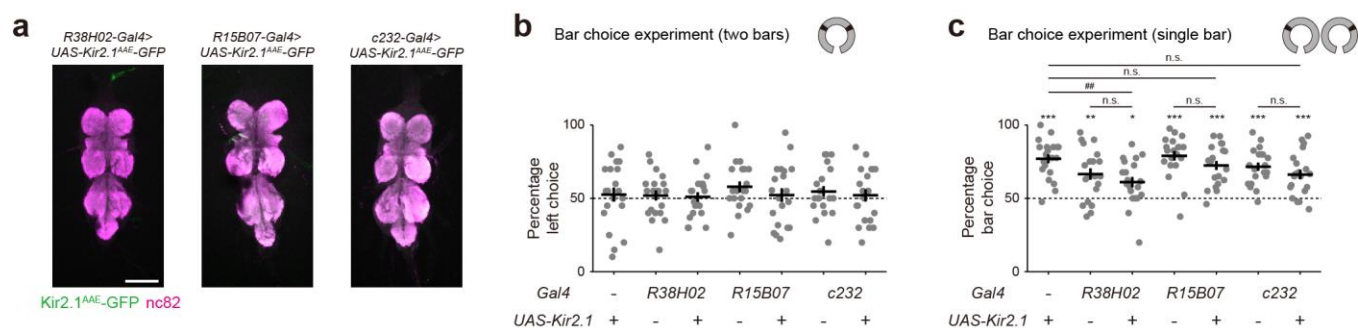**Supplementary Figure 1**

Characteristics of orientation behavior and the effects of a recent landmark.

(**a–c**) Bar choice experiment. (**a**) Task and stimuli. (**b**) Trajectories of the example fly shown in **Fig. 1e** during the choice period. One trial (gray line in the right panel) was discarded from further analyses (see Online Methods for the criteria for trial disposal). (**c**) Population summary (N = 20 flies). Each dot represents the percentage of "left" choice trials for a fly, calculated from 20 trials in each bar location. Choices were biased toward the bar side when one bar was presented (***$P < 0.001/2$, one-sample t-test with Bonferroni correction, the denominator represents the number of comparisons) but at random when two bars were simultaneously presented (Both, $P = 0.60$, one-sample t-test). Black lines, mean ± s.e.m. across flies. (**d**) Time course of trial-averaged ΔWBA during the cueing experiment shown in **Fig. 1d–f** (N = 20 flies, mean ± s.e.m. across flies). Inset is an enlarged view around the onset of the choice period. (**e**) Mean ΔWBA during the cue and the delay periods during the cueing experiment (N = 20 flies). Each dot represents the mean ΔWBA for a fly. Flies attempted to turn toward the cue during the cue period (***$P < 0.001$, one-sample t-test). Black lines, mean ± s.e.m. across flies. (**f,g**) Cue duration experiment. (**f**) Task. (**g**) Summary of choice bias for each cue duration (N = 20 flies). Same format as in **e** but the ordinate represents the percentage of trials in which the fly chose to orient toward the side where the cue had not been presented. *$P < 0.05/5$, **$P < 0.01/5$, ***$P < 0.001/5$, one-sample t-test with Bonferroni correction. (**h,i**) Delay duration experiment. (**h**) Task. (**i**) Summary of choice bias for each delay (N = 20 flies). Same format as in **g**. *$P < 0.05/4$, **$P < 0.01/4$, ***$P < 0.001/4$, one-sample t-test with Bonferroni correction. (**j–l**) Cueing and single bar location experiment. (**j**) Task. (**k**) Stimulus set. (**l**) Summary of choice bias for each condition (N = 20 flies). Same format as in **e** but the ordinate represents the percentage of trials in which the fly chose to orient toward the bar side. *$P < 0.05/3$, **$P < 0.01/3$, ***$P < 0.001/3$, one-sample t-test with Bonferroni correction. [#]$P < 0.05$, [###]$P < 0.001$, one-way analysis of variance (ANOVA) followed by post hoc Tukey's honestly significant difference (HSD) test. (**m,n**) Closed-loop cue experiment. (**m**) Task. (**n**) Summary of choice bias (N = 20 flies). Same format as in **g**. ***$P < 0.001$, one-sample t-test. (**o,p**) Cueing experiment with bright bars. (**o**) Task. (**p**) Summary of choice bias (N = 20 flies). Same format as in **g**. **$P < 0.01$, one-sample t-test. (**q,r**) Bar choice experiment with bright bars. (**q**) Task. (**r**) Summary of bar choice (N = 20 flies). Same format as in **l**. The choices were not different from the chance level ($P = 0.15$, one-sample t-test). (**s–u**) Bar location experiment. (**s**) Task. (**t**) Stimulus set. (**u**) Summary of choice bias for each bar location in the bar location experiment where only one bar was presented in the closed-loop mode at various locations (N = 20 flies). The degree of choice bias depended on bar location ($P < 0.001$, one-way ANOVA) with the strongest bias at ±60°. Same format as in **l**. **$P < 0.01/5$, ***$P < 0.001/5$, one-sample t-test with Bonferroni correction. (**v**) Mean ΔWBA during the cue and delay periods in cue/target location experiment shown in **Fig. 1g,h** (mean ± s.e.m. across flies; N = 20 flies for each combination of cue and target locations). These values were used to assess the motor hypothesis with partial correlation analysis (see Online Methods). Exact P values for all statistical tests can be found in **Supplementary Table 1**.

Supplementary Figure 2

Visually-guided flight orientation in flies with inactivated ring neurons.

(**a**) Expression patterns of the potassium channel in the ventral nerve cord of the three driver lines shown in **Fig. 2b**. Scale bar, 100 µm. (**b**) Summary of the choices in the bar choice experiment with two bars (N = 20 flies for each genotype). Each dot represents the percentage of trials in which the fly chose to orient toward the left side. Black lines, mean ± s.e.m. across flies. Variances of % "left" choice among flies did not depend on genotypes ($P > 0.05/3$ for all pairs of mutant and control genotypes, Bartlett's test with Bonferroni correction, the denominator represents the number of comparisons). (**c**) Summary of the choices in the bar choice experiment with a single bar (N = 20 flies for each genotype). The same format as in **b** but the ordinate represents the percentage of trials in which the fly chose to orient toward the bar side. $*P < 0.05/7$, $**P < 0.01/7$, $***P < 0.001/7$, one-sample t-test with Bonferroni correction. n.s., $P > 0.05/3$, $^{##}P < 0.01/3$, two-sample t-test with Bonferroni correction. Exact P values for all statistical tests can be found in **Supplementary Table 1**.
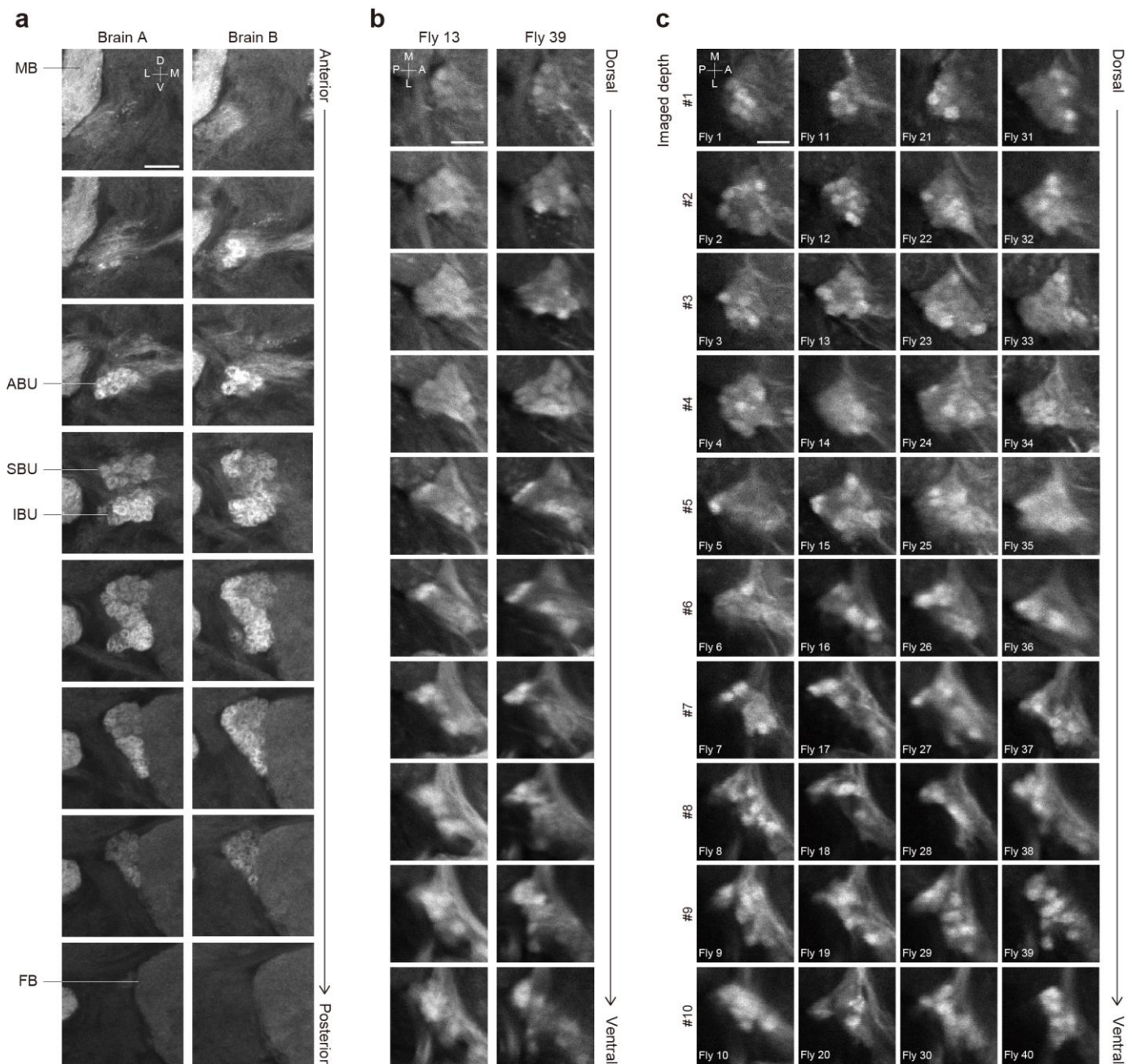
Supplementary Figure 3

**The structure of the BU is stereotyped across animals.**

(**a**) *In vitro* images of the BU in the right hemisphere of two brains. Images show the immunofluorescence of GFP in brains expressing GFP pan-neuronally. A confocal stack that covers the BU (48 frames, 24 μm) was divided into 8 subvolumes (6 frames, 3 μm). Each image is a projection of images in a subvolume. SBU, superior BU; IBU, inferior BU; ABU, anterior BU. MB, mushroom body; FB, fan-shaped body. Scale bar, 10 μm. (**b**) *In vivo* images of the BU in two flies expressing GCaMP6f pan-neuronally. A series of GCaMP6f images covering the BU (60 frames, 30 μm) was divided into 10 subvolumes (6 frames, 3 μm). Frames in a subvolume are averaged and normalized to obtain each image. Scale bar, 10 μm. (**c**) *In vivo* images of the recorded part of the BU in all flies used for calcium imaging experiments. Each image is obtained from a single fly by averaging 40 frames immediately before cue presentation in a trial. Images are grouped according to the depth of the target volume (see **Fig. 3f** for the location of target volumes). Scale bar, 10 μm.
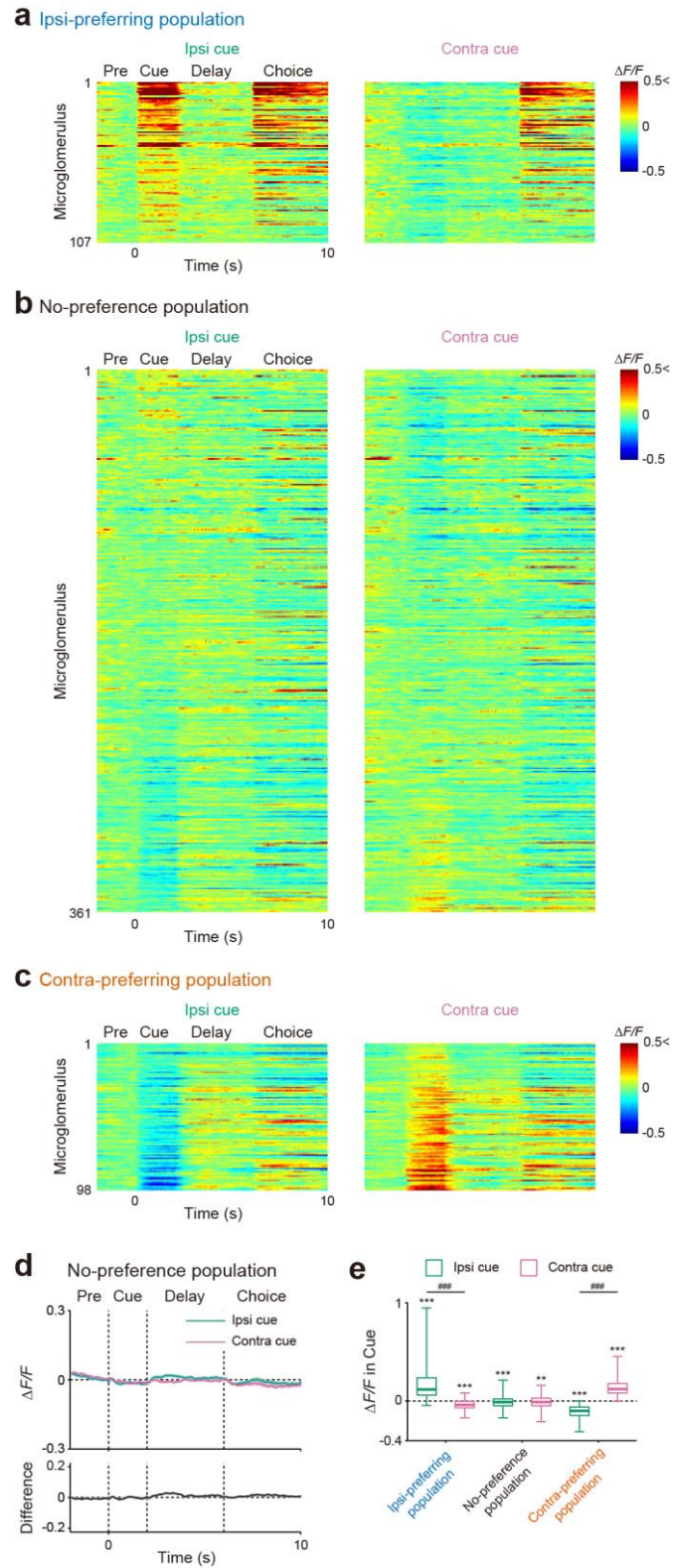
Supplementary Figure 4

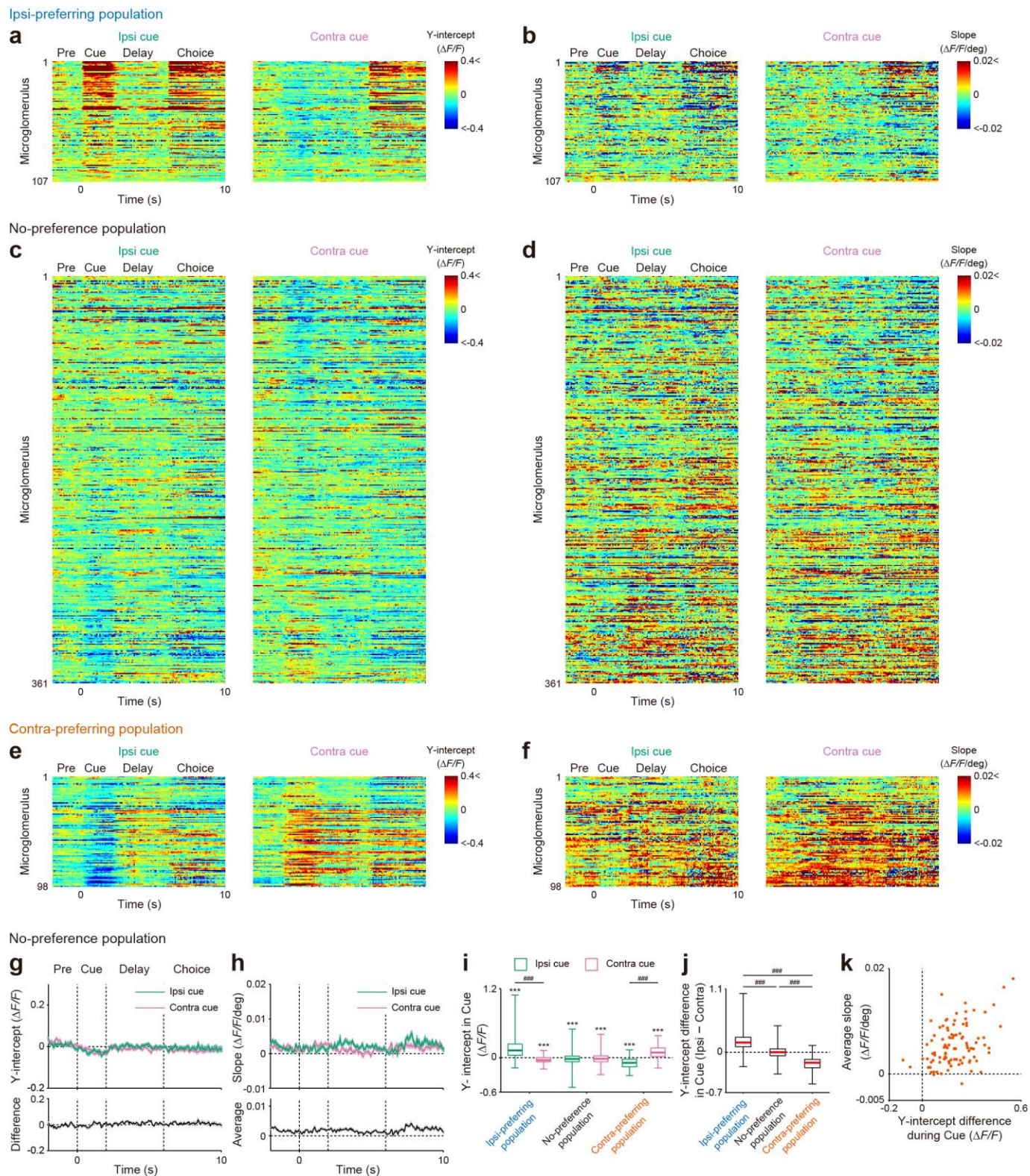**Activity of individual microglomeruli for each cue-location.**

(**a–c**) Each row represents the time course of the average *ΔF/F* of one microglomerulus. (**a**) Individual microglomeruli of the ipsi-preferring population (N = 107 microglomeruli in 21 flies). Microglomeruli are sorted according to the trial-type preference. (**b**) Same as in **a** but for the no-preference population (N = 361 microglomeruli in 40 flies). (**c**) Same as in **a** but for the contra-preferring population (N = 98 microglomeruli in 17 flies). (**d**) Population-averaged activity for each cue-location (mean ± s.e.m. across microglomeruli) for the the no-preference population. (**e**) Distribution of mean *ΔF/F* of each microglomerulus during the cue period. Box plots indicate median, quartiles, and range. **$P < 0.01/2$, ***$P < 0.001/2$, one-sample *t*-test with Bonferroni correction, the denominator represents the number of comparisons. ###$P < 0.001$, paired *t*-test. Exact P values for all statistical tests can be found in **Supplementary Table 1**.
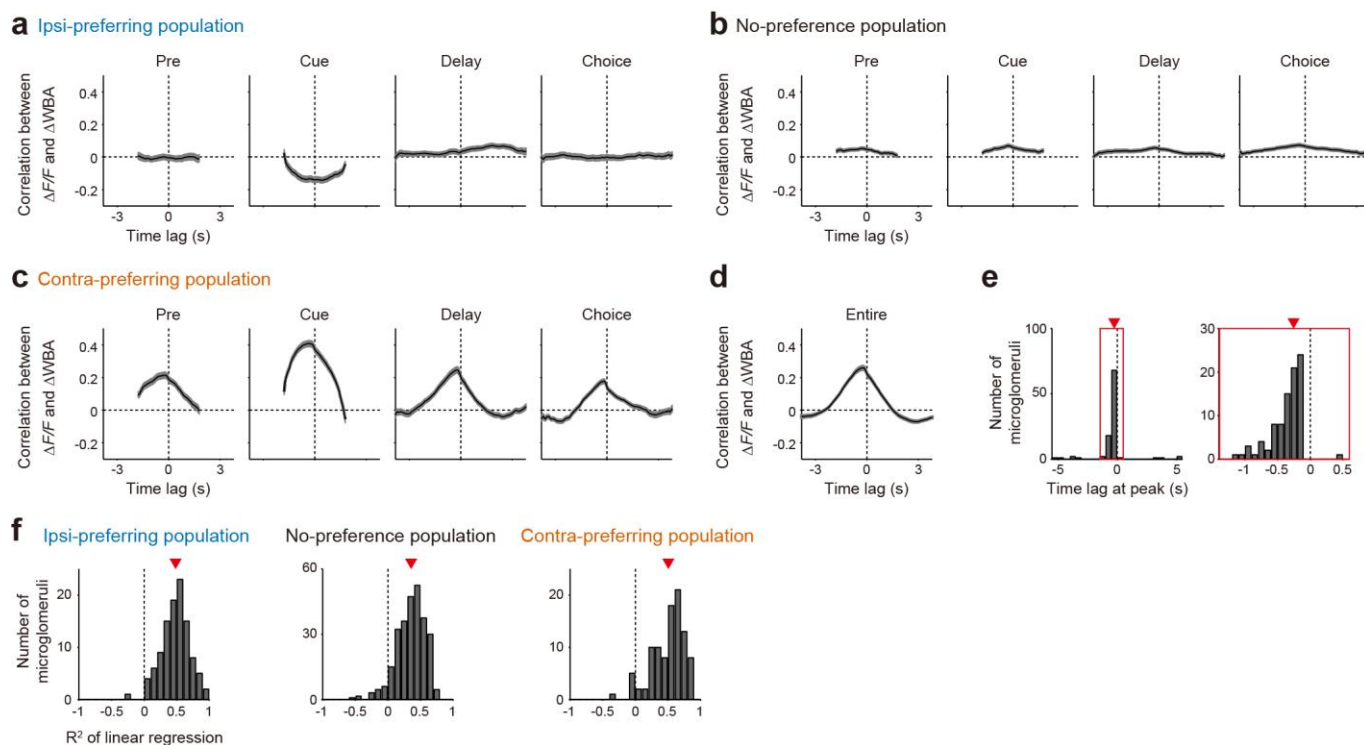
Supplementary Figure 5

**Construction and assessment of a linear regression analysis.**

A linear regression analysis of the activity of each microglomerulus was performed after taking into account the delay between calcium signals and intended turns using cross-correlation (see Online Methods). Cross-correlation between $\Delta F/F$ and ΔWBA was calculated separately for each task period (mean ± s.e.m. across microglomeruli) for the ipsi-preferring population (**a**) (N = 107 microglomeruli in 21 flies), the no-preference population (**b**) (N = 361 microglomeruli in 40 flies), and the contra-preferring population (**c**) (N = 98 microglomeruli in 17 flies). Positive correlations indicate higher activity for contralateral turns. Negative time lags represent the situations where changes in ΔWBA precede those in $\Delta F/F$. (**d**) Cross-correlation calculated based on the data from the entire task period for the contra-preferring population (mean ± s.e.m. across microglomeruli). (**e**) Histogram of the time lag at the peak of cross-correlation, calculated from the entire task period, for each microglomerulus of the contra-preferring population. Red triangles, median. This time lag was considered in the linear regression fit (see Online Methods). (**f**) Histogram of the quality of the linear regression fit quantified using R-squared. Red triangles, mean.

Supplementary Figure 6

**Regression parameters for individual microglomeruli.**

Time course of the Y-intercept (**a,c,e**) and the slope (**b,d,f**) in individual microglomeruli for each cue-location. Microglomeruli are sorted according to the trial-type preference in each population. (**a,b**) The ipsi-preferring population ($N = 107$ microglomeruli in 21 flies). (**c,d**) The no-preference population ($N = 361$ microglomeruli in 40 flies). (**e,f**) The contra-preferring population ($N = 98$ microglomeruli in 17 flies). (**g,h**) Time course of regression parameters (mean ± s.e.m. across microglomeruli) for the no-preference population. (**i**) Distribution of the average Y-intercept of each microglomerulus during the cue period, plotted separately for each cue-location and population. Box plots indicate median, quartiles, and range. ***$P < 0.001/2$, one-sample t-test with Bonferroni correction, the denominator represents the number of comparisons. ###$P < 0.001$, paired t-test. (**j**) Distribution of the difference in the average Y-intercepts between cue-locations during the cue period. Box plots indicate median, quartiles, and range. ***$P < 0.001$, one-way ANOVA followed by post hoc Tukey's HSD test. (**k**) Relationship between the average slope and the Y-intercept difference between cue-locations during the cue period for the contra-preferring population (Pearson's correlation coefficient, 0.41, $P < 0.001$). Each dot represents a microlomgerulus. Exact P values for all statistical tests can be found in **Supplementary Table 1**.
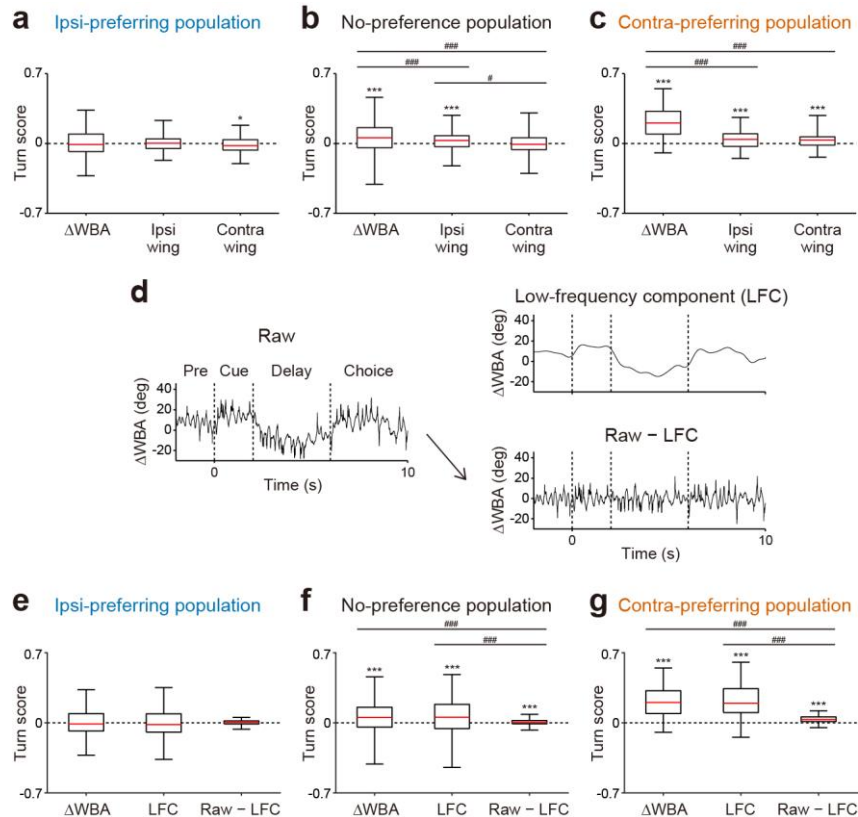
Supplementary Figure 7

**Slow changes in ΔWBA drive the turn-related component.**

(**a**) Distribution of turn scores calculated based on ΔWBA, the angle of ipsilateral wing, and that of contralateral wing for the ipsi-preferring population (N = 107 microglomeruli in 21 flies). Turn scores quantify the correlation between an aspect of wingbeat movement (e.g., ΔWBA) and the calcium signals corrected for the effect of cue-location (see Online Methods). Box plots indicate median, quartiles, and range. (**b**) Same as in **a** but for the no-preference population (N = 361 microglomeruli in 40 flies). (**c**) Same as in **a** but for the contra-preferring population (N = 98 microglomeruli in 17 flies). Turn scores based on ΔWBA were higher than those based on the angle of respective wings. (**d**) Raw ΔWBA traces were low-pass filtered to separate the low-frequency component (LFC) from the high-frequency component (Raw − LFC). (**e**) Same as in **a** but for ΔWBA, the LFC of ΔWBA, and the Raw − LFC. (**f**) Same as in **e** but for the no-preference population. (**g**) Same as in **e** but for the contra-preferring population. Turn scores based on ΔWBA and the LFC were higher than those for the Raw − LFC. *P < 0.05/3, ***P < 0.001/3, one-sample t-test with Bonferroni correction, the denominator represents the number of comparisons. #P < 0.05, ###P < 0.001, one-way ANOVA followed by post hoc Tukey's HSD test. Exact P values for all statistical tests can be found in **Supplementary Table 1**.
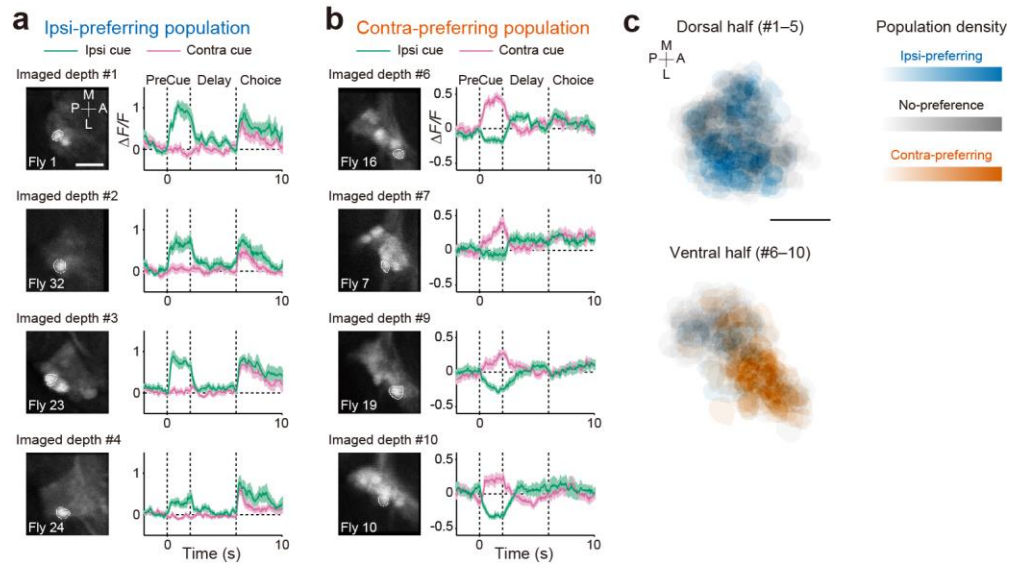
Supplementary Figure 8

**Distribution of the ipsi-preferring and the contra-preferring populations.**

(**a**) Four example microglomeruli located in the dBU. Images were generated by averaging frames of highest intensity (top 5%) for each microglomerulus. Traces indicate the time course of calcium signals for each cue-location (mean ± s.e.m. across trials). Scale bar, 10 µm. (**b**) Same as in **a** but for four other examples located in the vBU. (**c**) Density of each population in the dBU and the vBU. Images were generated based on the contours of microglomeruli in each recording (e.g., left panel in **Fig. 3e**). No image registration was performed across brains because we recorded from highly consistent areas across brains (**Supplementary Fig. 3c**). Scale bar, 10 µm.
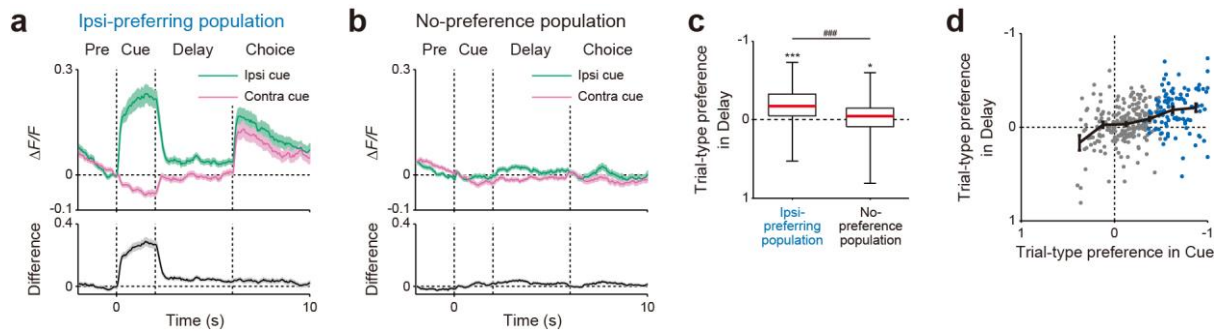
Supplementary Figure 9

Microglomeruli in the dBU showing stronger cue responses also show stronger delay-period activity.

(**a**) Population-averaged activity for each cue-location for the ipsi-preferring population in the dBU (N = 98 microglomeruli in 19 flies; mean ± s.e.m. across microglomeruli). (**b**) Same as in **a** but for the no-preference population in the dBU (N = 220 microglomeruli in 20 flies). (**c**) Distributions of the trial-type preference calculated based on $\Delta F/F$ in the last 3 s of the delay period, which quantifies the selectivity for cue-location in this period of activity (see Online Methods). Box plots indicate median, quartiles, and range. The mean trial-type preference in the delay period for the ipsi-preferring population was -0.18 ± 0.02 (mean ± s.e.m., N = 98 microglomeruli; corresponding to the percentage of correct discrimination of 59.0 ± 1.1%), which was more reliable than the choice bias of the flies during the recording (the percentage of uncued choice, 56.3 ± 1.5%, mean ± s.e.m., N = 20 flies). Note that the ordinate is reversed so that values representing higher activity in the ipsilateral cue trials are plotted in the upper part. *$P < 0.05$, ***$P < 0.001$, one-sample t-test. ###$P < 0.001$, two-sample t-test. (**d**) Relationship between the trial-type preferences calculated based on $\Delta F/F$ in the cue period and those calculated based on $\Delta F/F$ in the last 3 s of the delay period (Pearson's correlation coefficient, 0.38, $P < 0.001$). Each dot represents a microglomerulus (blue, the ipsi-preferring population; gray, the no-preference population). Black lines indicate the population summary of the trial-type preference in the last 3 s of the delay period (mean ± s.e.m. across microglomeruli) calculated every 0.2 of the trial-type preference in the cue period. Exact p-values for all statistical tests can be found in **Supplementary Table 1**.
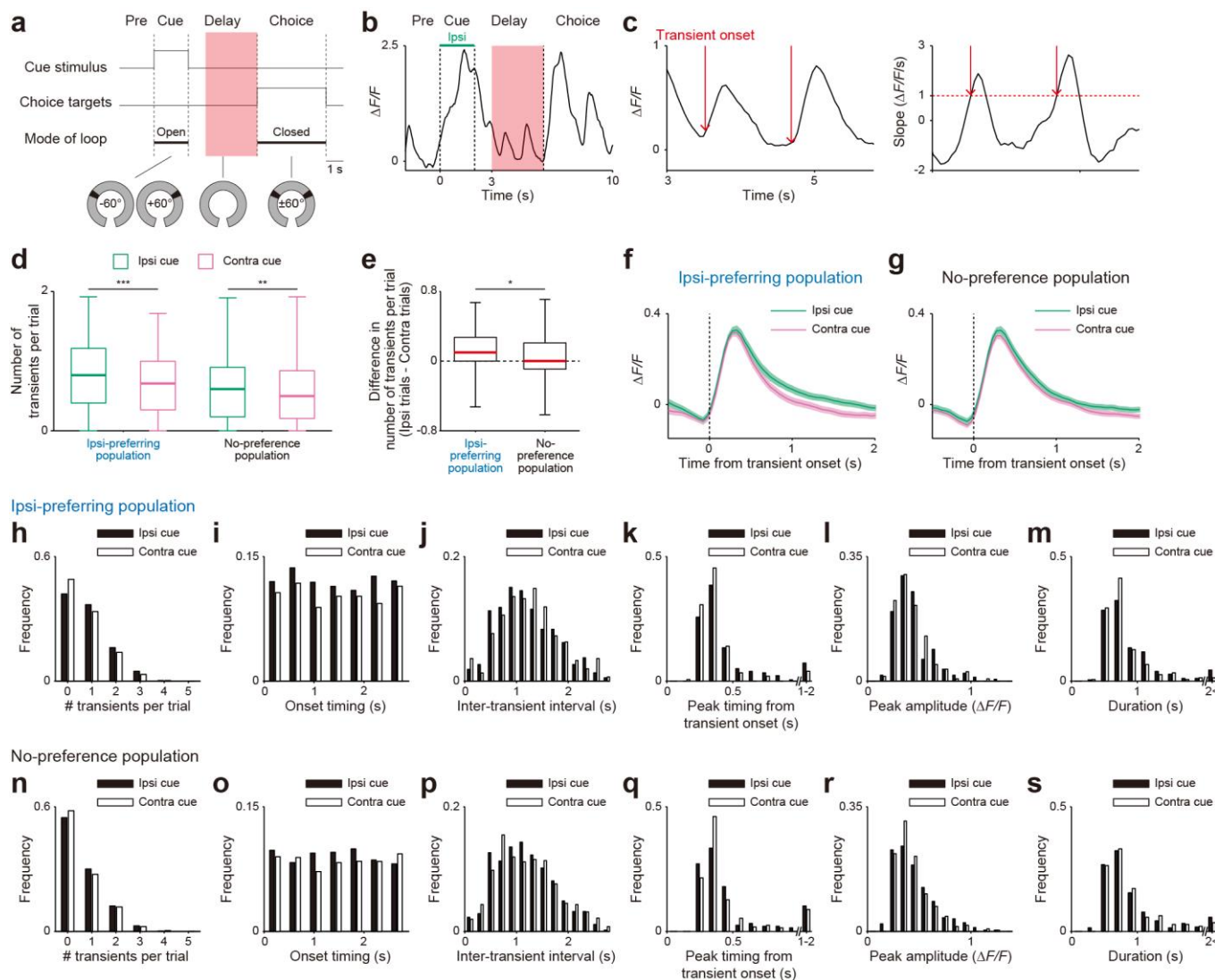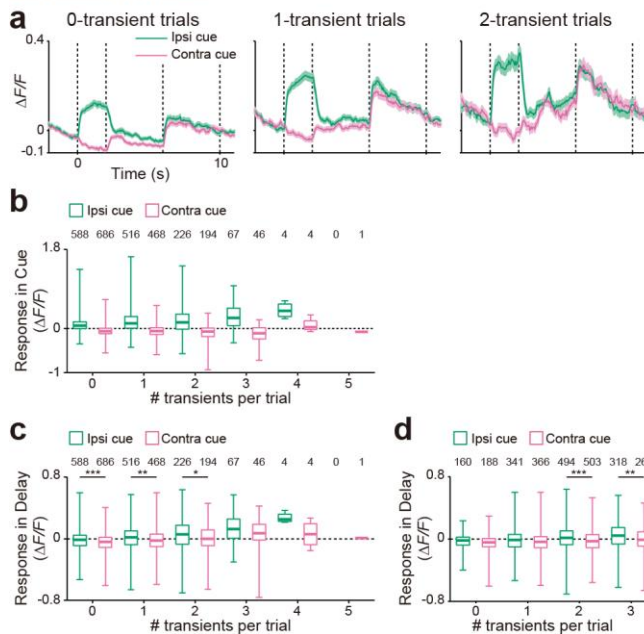
Supplementary Figure 10

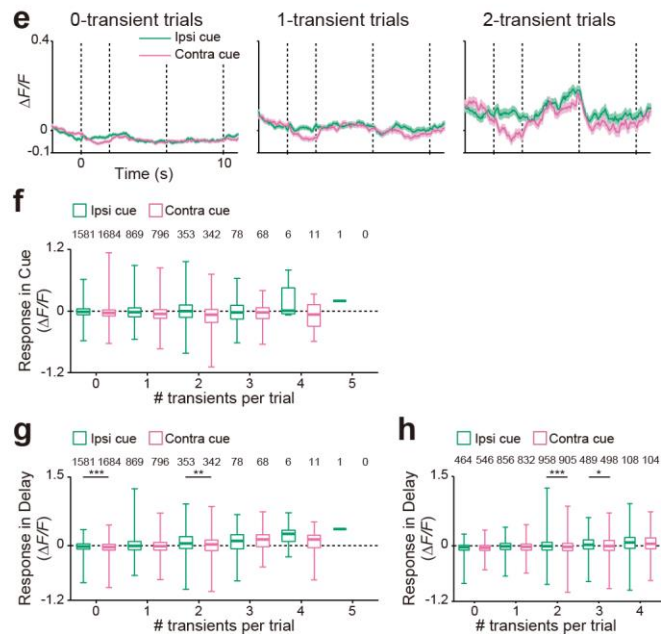**Delay-period activity in the dBU is composed of calcium transients.**

(**a**) Analyses were based on the data in the last 3 s of the delay period (red). (**b**) Time course of calcium signals in an ipsilateral cue trial from the example microglomerulus shown in **Fig. 3g,h**. Calcium signals were filtered with a boxcar filter of 5 frames (255 ms). (**c**) Detection of calcium transients. Left, magnified view of the trace in **b**. Right, time derivative of the calcium signal. Arrows indicate the onset of calcium transients, defined as the time the derivative exceeds a threshold (1 *ΔF/F*/s, dotted line in the right panel). (**d**) Distribution of the mean number of transients per trial plotted separately for each cue and population in the dBU (the ipsi-preferring population, *N* = 98 microglomeruli in 19 flies; the no-preference population, *N* = 220 microglomeruli in 20 flies). Box plots indicate median, quartiles, and range. **P < 0.01, ***P < 0.001, paired *t*-test. (**e**) Same as in **d** but for the difference in the mean number of transients between ipsilateral and contralateral cue trials. *P < 0.05, two-sample *t*-test. (**f–s**) Characteristics of calcium transients during the delay period for the ipsi-preferring population (**f,h–m**) and the no-preference population (**g,n–s**). (**f,g**) Time course of transients averaged across trials (mean ± s.e.m.). Analyses were done on trials with just one transient occurring in the last 3-s of the delay period with its onset in the first 1 s of the analyzed period (*N* = 179 ipsilateral and 150 contralateral cue trials for the ipsi-preferring population, *N* = 284 ipsilateral and 284 contralateral cue trials for the no-preference population). The same sets of trials were used in **k–m,q–s**. (**h,i,n,o**) Histogram of the number of transients (**h,n**) and onset timing (**i,o**) (*N* = 1401 ipsilateral and 1399 contralateral cue trials for the ipsi-preferring population, *N* = 2888 ipsilateral and 2901 contralateral cue trials for the no-preference population). (**j,p**) Histogram of inter-transient interval calculated from trials with more than one transients (*N* = 297 ipsilateral and 245 contralateral cue trials for the ipsi-preferring population, *N* = 438 ipsilateral and 421 contralateral cue trials for the no-preference population). (**k,q**) Histogram of the peak timing from transient for onset. (**l,r**) Histogram of the peak amplitude. (**m,s**) Histogram of transient duration (see Online Methods for

the definition of the duration). Exact *P* values for all statistical tests can be found in **Supplementary Table 1**.

Supplementary Figure 11

Delay-period activity in the dBU may contain persistent as well as transient components.

(**a–d**) The ipsi-preferring population (*N* = 98 microglomeruli in 19 flies). (**a**) Time course of calcium signals for each cue-location plotted separately for the number of calcium transients in the last 3 s of the delay period. The number of trials is indicated in **b**. (**b**) Distributions of responses in the cue period for each cue-location and the number of transients per trial. Responses were defined as the difference in mean *ΔF/F* between the 2-s pre-cue period and the cue period. Box plots indicate median, quartiles, and range. Numbers above the box plots indicate the number of trials in each condition. Stronger cue responses were followed by a larger number of transients in ipsilateral cue trials (Pearson's correlation coefficient, 0.19, *P* < 0.001) whereas by a slightly lower number of transients in contralateral cue trials (Pearson's correlation coefficient, -0.065, *P* = 0.015). (**c**) Same as in **b** but for responses in the last 3 s of the delay period. Responses in the delay period increased with the number of transients per trial (Pearson's correlation coefficient; ipsilateral cue trials, 0.24, *P* < 0.001; contralateral cue trials, 0.18, *P* < 0.001). **P* < 0.05/3, ***P* < 0.01/3, ****P* < 0.001/3, paired *t*-test with Bonferroni correction, the denominator represents the number of comparisons. Tests were performed when the number of trials exceeded 100 trials for both cue-locations. (**d**) Same as in **c** but for a lower threshold for defining transients (see Online Methods). Data are shown for conditions where the number of trials exceeded 100 for both cues. ***P* < 0.01/4, ****P* < 0.001/4. (**e–h**) Same as in **a–d** but for the no-preference population (*N* = 220 microglomeruli in 20 flies). (**f**) Stronger cue responses were followed by a minutely larger number of transients per trial in ipsilateral cue trials (Pearson's correlation coefficient, 0.037, *P* = 0.049) and by a lower number of transients in contralateral cue trials (Pearson's correlation coefficient, -0.11, *P* < 0.001). (**g**) Responses in the delay period increased with the number of transients per trial (Pearson's correlation coefficient; ipsilateral cue trials, 0.18, *P* < 0.001; contralateral cue trials, 0.15, *P* < 0.001). ***P* < 0.01/3, ****P* < 0.001/3, paired *t*-test with Bonferroni correction. (**h**) **P* < 0.05/5, ****P* < 0.001/5, paired *t*-test with Bonferroni correction. Exact *P* values for all statistical tests can be found in **Supplementary Table 1**.
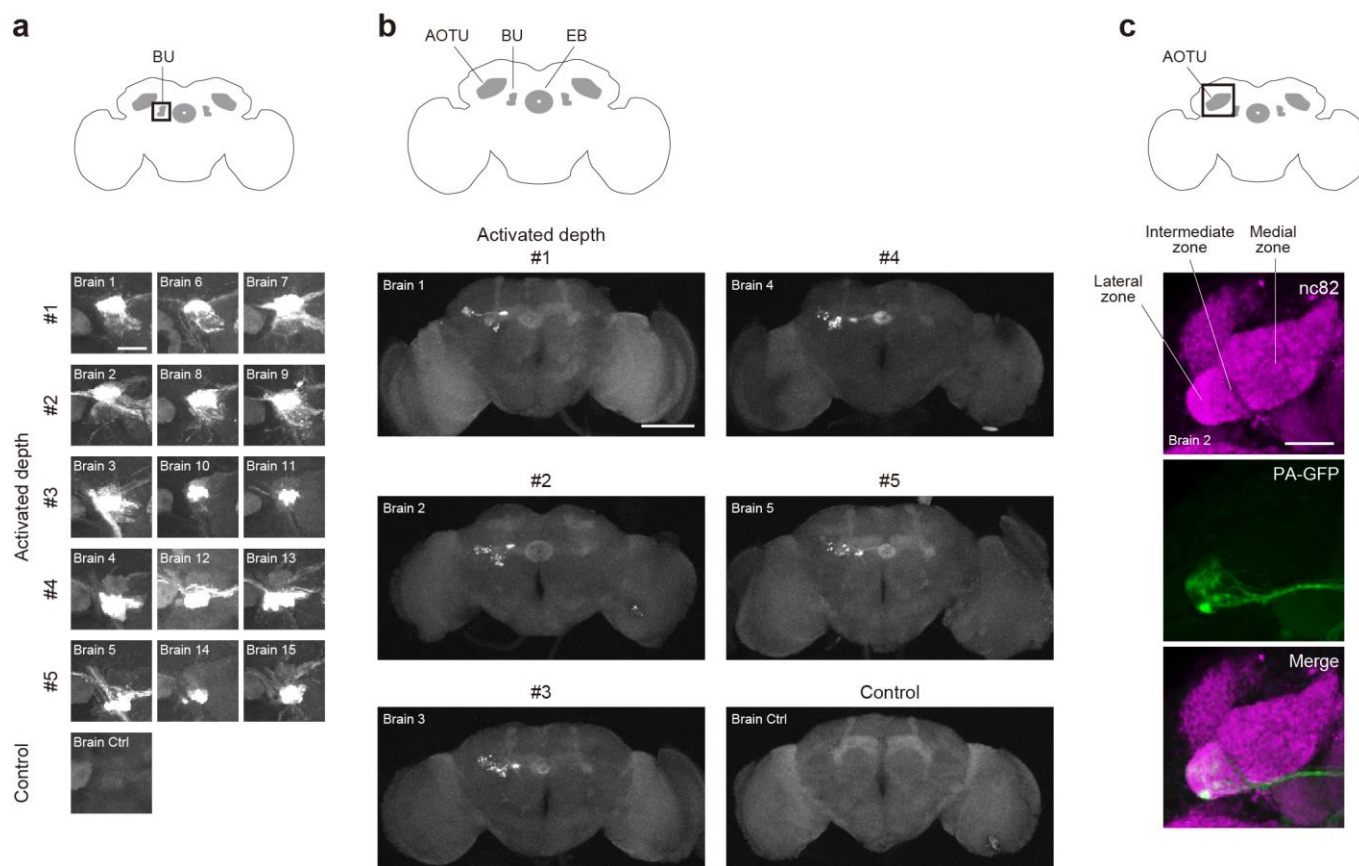
Supplementary Figure 12

Localization of PA-GFP photolabeling.

(**a**) Photoactivation of a volume of the BU at one of the five depths along the dorsal-ventral axis (3 brains for each depth; see **Fig. 6b** for the location of target volumes). Each image is a projection of a confocal stack that covers the BU. No photoactivation was applied to the control brain. Top: schematic of the imaged region of the brain. Scale bar, 20 μm. (**b**) Whole-brain photolabeling patterns of brains shown in **Fig. 6**. Each image is a projection of a confocal stack covering the brain. Top: schematic of the fly brain. Scale bar, 100 μm. (**c**) Photolabeling in the AOTU of a representative brain. Images are projections of a confocal stack covering the AOTU. The AOTU is composed of medial, intermediate, and lateral zones (top image). Top: schematic of the imaged region of the brain. Magenta, nc82; green, PA-GFP. Scale bar, 20 μm.
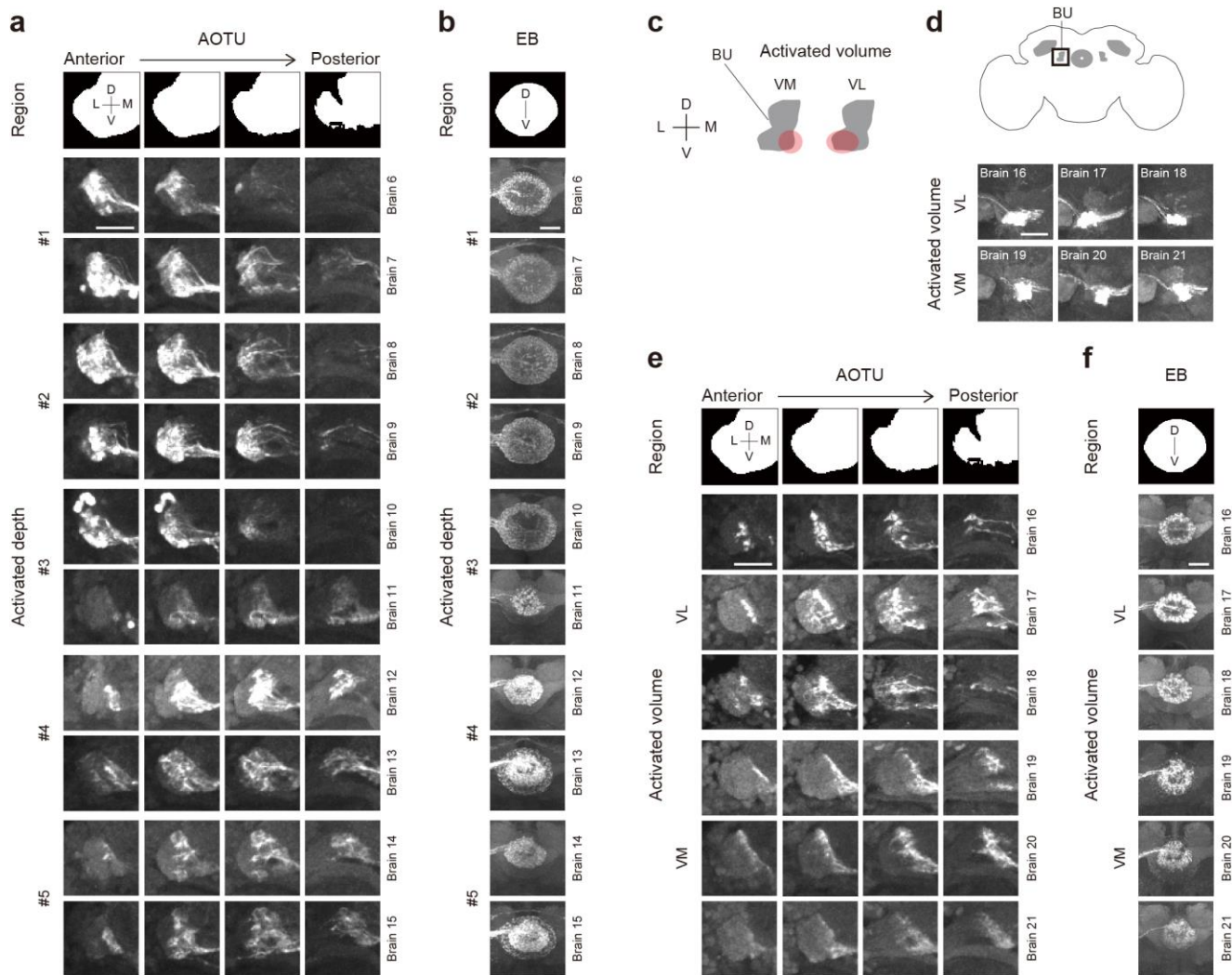
Supplementary Figure 13

Photolabeling in other PA-GFP experiments.

(**a,b**) Photolabeling in the EB (**a**) and the AOTU (**b**) in brains not shown in **Fig. 6** in which a volume of the BU was photoactivated at one of the five depths along the dorsal-ventral axis (2 brains for each depth; see **Fig. 6b** for the location of target volumes). Each image is a projection of a confocal stack covering a subvolume of the AOTU (**a**) or the EB (**b**) as in **Fig. 6d,e**. Top: regions of the target brain structures in a standard brain. Scale bars, 20 μm. (**c–f**) Photoactivation of the ventromedial (VM) or the ventrolateral (VL) parts of the BU. (**c**) Schematic of photoactivated volumes (red). (**d**) Photolabeling in the BU for VL and VM photoactivation (3 brains for each volume). Each image is a projection of a confocal stack covering the BU. Top: schematic of the imaged region of the brain. Scale bars, 20 μm. (**e,f**) Same as in **a,b** but for VL and VM photoactivation.
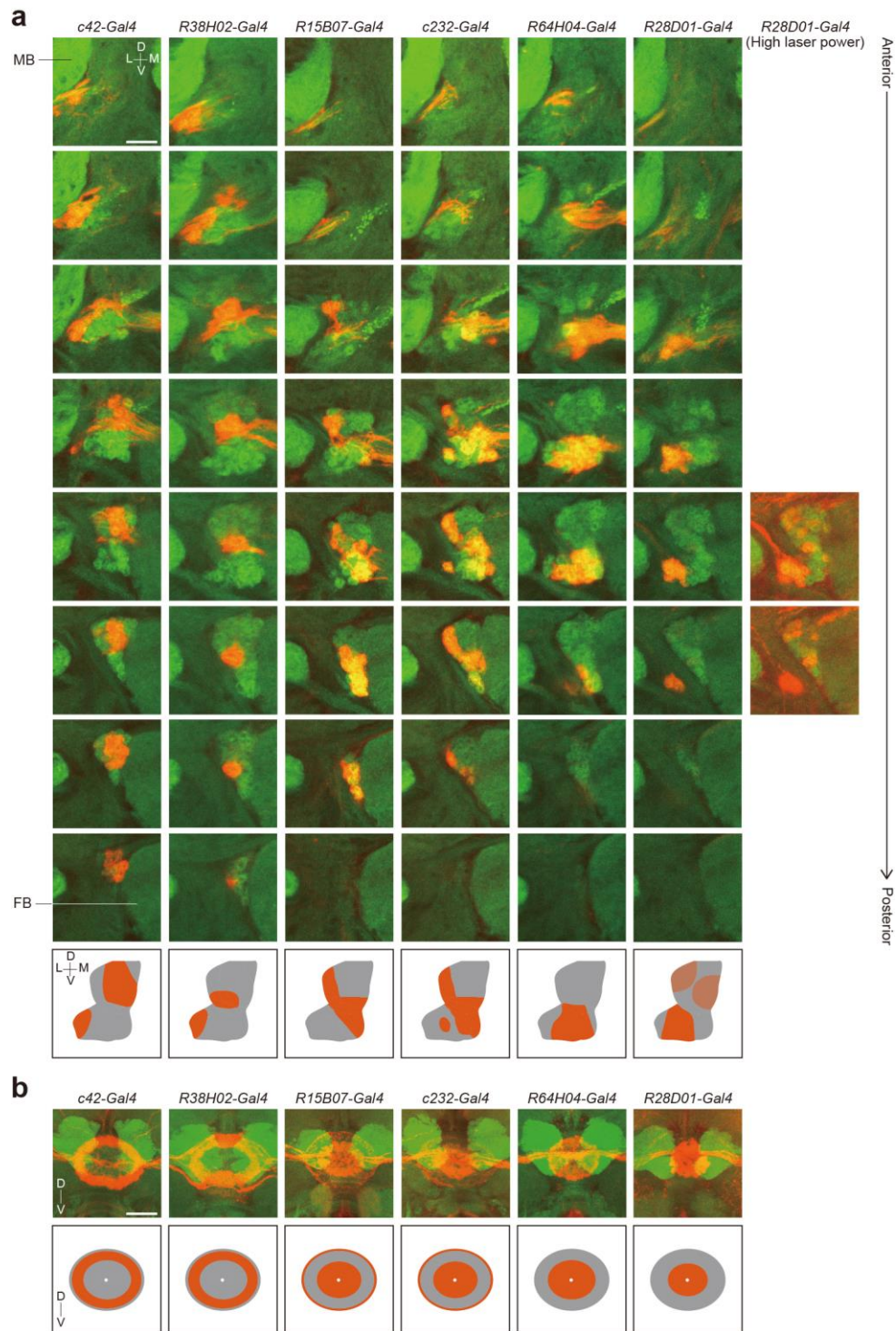
Supplementary Figure 14

Different types of ring neurons innervate different parts of the BU.

(**a**) Gal4-expression patterns in the BU of the right hemisphere. Images show the immunofluorescence of GFP (green) expressed using a pan-neuronal driver line and the red fluorescent protein (RFP, orange) expressed using driver lines specific to type(s) of ring neurons. Each image is a projection of a confocal stack that covers a subvolume of the BU (6 frames, 3 μm). Scale bar, 10 μm. Bottom panels show schematics of the region of the BU labeled. *c42-Gal4* labels R2 and R4 neurons[34], *R38H02-Gal4* labels R4 neurons[11], *R15B07-*

Gal4 labels R1 and R4 neurons[11], *c232-Gal4* labels R3 and R4d neurons[34], *R64H04-Gal4* labels R3 neurons, and *R28D01-Gal4* labels R1 neurons[11]. *R28D01-Gal4* also labeled microglomeruli in the dBU weakly, which was visible with a strong laser (the rightmost column). The labeling of some of these microglomeruli extended to the AOTU (data not shown). (**b**) Gal4-expression patterns in the EB. Each image is a projection of a confocal stack covering the EB. Scale bar, 20 µm.

Figure	Genotype
1 and S1	Wild-type
2 and S2	*UAS-Kir2.1^{AAE}-GFP/+*
	R38H02-Gal4(attP2)/ +
	R38H02-Gal4(attP2)/ UAS-Kir2.1^{AAE}-GFP
	R15B07-Gal4(attP2)/ +
	R15B07-Gal4(attP2)/ UAS-Kir2.1^{AAE}-GFP
	c232-Gal4/ +
	c232-Gal4/ UAS-Kir2.1^{AAE}-GFP
3a,b and S3a	*UAS-IVS-mCD8::GFP(attP40)/+;R57C10-Gal4(attP2)/+*
3e–o, 4, 5, S3b,c, and S4 to S11	*UAS-IVS-GCaMP6f(attP40);R57C10-Gal4(attP2)*
6, S12, and S13	*R57C10-Gal4(attP2)/UAS-IVS-Syn21-mC3PA-GFP-p10(attP2),UAS-IVS-Syn21-mC3PA-GFP-p10(VK00005)*
S14	*UAS-IVS-mCD8::RFP(attP18),LexAop2-mCD8::GFP(attP8)/+;R57C10-lexA(attP40)/+;c42-Gal4/+*
	UAS-IVS-mCD8::RFP(attP18),LexAop2-mCD8::GFP(attP8)/+;R57C10-lexA(attP40)/+;R38H02-Gal4(attP2)/+
	UAS-IVS-mCD8::RFP(attP18),LexAop2-mCD8::GFP(attP8)/+;R57C10-lexA(attP40)/+;R15B07-Gal4(attP2)/+
	UAS-IVS-mCD8::RFP(attP18),LexAop2-mCD8::GFP(attP8)/+;R57C10-lexA(attP40)/+;c232-Gal4/+
	UAS-IVS-mCD8::RFP(attP18),LexAop2-mCD8::GFP(attP8)/+;R57C10-lexA(attP40)/+;R64H04-Gal4(attP2)/+
	UAS-IVS-mCD8::RFP(attP18),LexAop2-mCD8::GFP(attP8)/+;R57C10-lexA(attP40)/+;R28D01-Gal4(attP2)/+

Supplementary Table 1 Genotypes of flies used in this study.